DOI: 10.1002/ejic.201001340

# Asymmetrically Dibridged Diiron(III) Complexes with Aminebis(phenoxide)-Based Ligands for a Magnetostructural Study

**Thomas Weyhermüller,[a] Rita Wagner,[a] and Phalguni Chaudhuri*[a]**

**Keywords:** Transition metals / Iron / Magnetic properties / N,O ligands / Through-bond interactions

The ligands [*N*,*N*-bis(3,5-di-*tert*-butyl-2-hydroxybenzyl)aminoacetic acid] ($H_3L^1$), [*N*,*N*-bis(2-hydroxy-3,5-dimethylbenzyl)-aminoacetic acid] ($H_3L^2$), [*N*,*N*-bis(2-hydroxy-3,5-dimethylbenzyl)-*N*-(2-pyridylmethyl)amine] ($H_2L^3$) and [methylamino-*N*,*N*-bis(6-*tert*-butyl-4-methyl-2-methylenephenol)] ($H_2L^4$) were used to investigate their coordination properties toward $Fe^{III}$. The ligand $H_3L^1$ yields mononuclear iron(III) complexes, complexes **1**–**3**, whereas the asymmetrically dibridged diiron(III) complexes **4**–**8** were isolated with the ligands $H_3L^2$, $H_2L^3$ and $H_2L^4$. The complexes **1**–**8** have been structurally, magnetochemically (2–290 K) and spectroscopically investigated. Presumably as an effect of the sterically demanding *tert*-butyl groups, only mononuclear $Fe^{III}$ complexes **1**–**3** were isolated with $H_3L^1$, whereas $H_3L^2$ bearing the less bulky methyl groups results in the diferric(III) complex **4**. Complexes **4**–**8**, containing two $d^5$ high-spin ferric centres, possess a diamagnetic $S_t = 0$ ground state that is attained through intramolecular antiferromagnetic coupling between the two paramagnetic centres. We have focused our investigation largely on the magnetostructural correlation of the asymmetrically dibridged (hydroxo, methoxo, acetate) diferric(III) complexes **4**–**8** and compared these to similar compounds reported in the literature. The spin-exchange ability of the groups such as –OH, –OMe, –OR and –OPh is also compared.

## Introduction

The study of complexes with phenol-containing ligands is of unabated interest to inorganic chemists because of their relevance to apparently dissimilar fields, such as bioinorganic chemistry,[1] molecular magnetism[2] and catalysis.[3] Thus, aminebis(phenolate) ligands (potential O,N,O donors) have attracted the attention of researchers for use in the field of phosphorus chemistry[4] and for catalytic olefin polymerisation involving group IV metal complexes;[5] we have used such ligands in the field of transition metal chemistry.[6] With an aim to scrutinise the effect of an additional pendent arm (containing a donor atom) on the ligating property of the resulting tetradentate ligand towards late transition metal ions, particularly iron, we argued for a carboxylate and a pyridine donor group. Additionally, we wished to extend our investigations on the effect of steric hindrance of the resulting tripodal ligands by substituting the methyl groups on the phenol rings by *tert*-butyl groups. Thus, the ligands [*N*,*N*-bis(3,5-di-*tert*-butyl-2-hydroxybenzyl)aminoacetic acid] ($H_3L^1$), [*N*,*N*-bis(2-hydroxy-3,5-dimethylbenzyl)aminoacetic acid] ($H_3L^2$), [*N*,*N*-bis(2-hydroxy-3,5-dimethylbenzyl)-*N*-(2-pyridylmethyl)amine] ($H_2L^3$) and [methylamino-*N*,*N*-bis(6-*tert*-butyl-4-methyl-2-methylenephenol)] ($H_2L^4$) were selected for the investigations (Scheme 1).

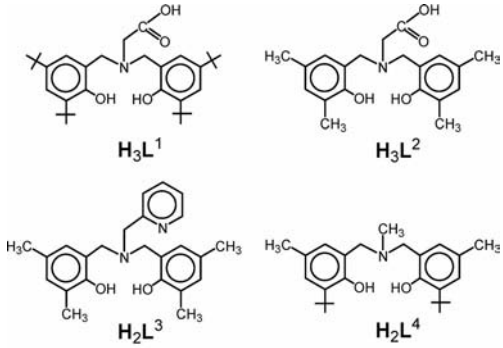


| | |
|---|---|
| $[(L^1)Fe^{III}(OH_2)]$ | complex **1** |
| $[(L^1)Fe^{III}(EtOH)]$ | complex **2** |
| $[Et_3NH][(L^1)Fe^{III}(OMe)]$ | complex **3** |
| $[Et_3NH][(L^2)_2Fe^{III}{}_2(\mu\text{-}OH)(OH_2)]$ | complex **4** |
| $[(L^3)_2Fe^{III}{}_2(\mu\text{-}OH)_2]$ | complex **5** |
| $[(L^3)_2Fe^{III}{}_2(\mu\text{-}OCH_3)(\mu\text{-}OOCCH_3)]$ | complex **6** |
| $[(L^4)_2Fe^{III}{}_2(\mu\text{-}OH)_2]$ | complex **7** |
| $[(L^4)_2Fe^{III}{}_2(MeOH)(\mu\text{-}OH)(\mu\text{-}OMe)]$ | complex **8** |

Scheme 1.

[a] Max Planck Institute for Bioinorganic Chemistry,
Stiftstraße 34-36, 45470 Mülheim an der Ruhr, Germany
Fax: +49-208-306-3951
E-mail: chaudhuri@mpi-muelheim-mpg.de

Supporting information for this article is available on the WWW under http://dx.doi.org/10.1002/ejic.201001340.

  

We herein report the isolation, and structural and magnetochemical characterisation of complexes **1**–**8** with a special focus on the magnetostructural correlation of the asymmetrically dibridged diiron(III) complexes **4**–**8**.

## Results and Discussion

The ligands $H_3L^1$, $H_3L^2$, $H_2L^3$ and $H_2L^4$ were prepared by a one-pot Michael condensation reaction according to a modified procedure reported in the literature.[4,5a] The purity of the ligands was confirmed by liquid chromatography to be >98%. The IR and $^1$H NMR spectroscopic and MS data (see Exp. Section) are in agreement with the available literature data and hence no further discussion is necessary here.

Methanolic solutions of the ligands were treated with different iron salts and $Et_3N$ in suitable ratios and the solutions were heated to reflux to yield complexes **1**–**8** in reasonable yields. Depending on the nature of the metal salts, different products were isolated.

Selected IR data for complexes **1**–**8** are given in the Exp. Section. The peaks that convey most information are ν(OH), which are very sharp in the pure ligands, occurring in the 3629–3125 cm$^{-1}$ region, and vanish after complex formation indicating that the phenol character of the ligands has been lost. Complexes **1**–**4** exhibit strong to moderate vibrations between 1655–1617 ($\nu_{as}$OCO), 1476–1470 ($\nu_s$OCO) and 857–840 cm$^{-1}$ ($\nu_\delta$OCO) as observed earlier for carboxylato complexes.[11] For complexes **5** and **6**, the vibrations of the pyridine ring occur at 1445 and 1450 cm$^{-1}$, respectively. There are several peaks in the 3000–2800 cm$^{-1}$ region due to the ν(C–H) vibrations found in the normal range for methyl and *tert*-butyl groups.

Although mass spectrometric measurements do not leave any doubt about the mononuclearity for complexes **1**–**3** and dinuclearity for complexes **4**–**8**, unambiguous detailed characterisation providing atom-connectivity could not be obtained from the MS data. Selected MS data for the complexes are given in the Experimental Section.

### X-ray Diffraction Studies

Single crystals of deep brown $[(L^1)Fe(OH_2)]$ (**1**), $[(L^1)Fe(C_2H_5OH)]$ (**2**) and $[(L^1)Fe(OCH_3)][(C_2H_5)_3NH]$ (**3**) were obtained either from a methanol or ethanol solution by slow evaporation at ambient temperature. As the molecular structures of neutral **1**, **2** and the anion in **3** are very similar, we confine our discussion only to that of **3**. Pertinent crystallographic data for all three compounds are summarised in Table 8. An ORTEP diagram of **3** is shown in Figure 1 and selected bond lengths and angles are summarised in Table 1. The corresponding information for compounds **1** and **2** can be found in Figures S1 and S2, and Tables S1 and S2, respectively, in the Supporting Information.

The structure of **3** consists of one $[(L^1)Fe(OCH_3)]^-$ anion, one non-coordinated $[(C_2H_5)_3NH]^+$ cation and a methanol molecule of crystallisation. The overall geometry around the Fe(1) centre is best described as a distorted trigonal bipyramid with N(8) of $[L^1]^{3-}$ and O(40) of the methoxide ion as the apices; the N(8)–Fe(1)–O(40) angle is 161.88(7)°. The trigonality index[12] $\tau = [(\phi_1 - \phi_2)/60]$, in which $\phi_1$ and $\phi_2$ are the two largest L–M–L angles of the coordination sphere, has been calculated for Fe(1) to be 0.573 for **3** ($\tau$ = 1 for a perfect trigonal bipyramid and $\tau$ = 0 for a perfect square pyramid). The corresponding $\tau$ values for **1** and **2** are 0.715 and 0.679, respectively, confirming the distorted trigonal bipyramidal character of both iron centres. The bond length between the $Fe^{III}$ ion and the tertiary apical nitrogen atom N(8), which is situated trans to the methoxide oxygen O(40), of 2.2343(14) Å is about 0.06 Å longer for **3** than the distances between Fe(1) and the neutral oxygen atoms, originating from EtOH for **2** and $H_2O$ for **1**, as is expected. Accordingly, the Fe(1)–O(40) bond length is shorter for **3** [1.912(2) Å] than the corresponding $Fe^{III}$–O bonds in **1** and **2** and falls in the range of bond lengths previously determined for terminally bound methoxides in structurally characterised $Fe^{III}$ complexes.[13] The phenolates O(15) and O(1), together with the carboxylate oxygen O(18), define the equatorial plane of the five-coordinate Fe(1). The $FeNO_4$ coordination sphere is not very com-

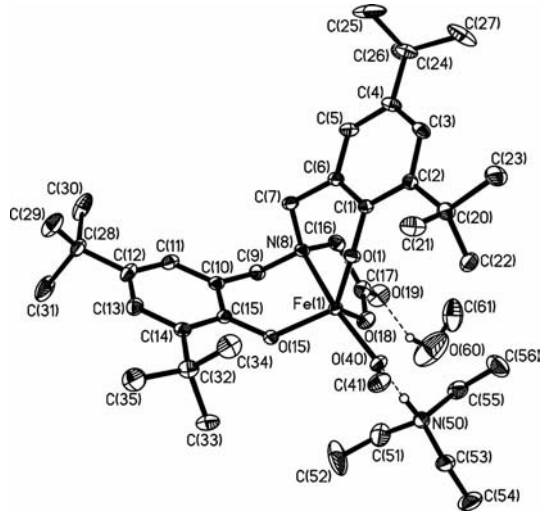


Figure 1. ORTEP diagram of **3** with ellipsoids drawn at the 40% probability level.

Table 1. Bond lengths [Å] and angles [°] for **3**·$CH_3OH$.

| | |
|---|---|
| Fe(1)–O(1) | 1.8782(12) |
| Fe(1)–O(15) | 1.8802(13) |
| Fe(1)–O(40) | 1.9118(12) |
| Fe(1)–O(18) | 1.9937(14) |
| Fe(1)–N(8) | 2.2343(14) |
| O(1)–C(1) | 1.3503(19) |
| O(15)–C(15) | 1.344(2) |
| O(1)–Fe(1)–O(15) | 112.71(6) |
| O(1)–Fe(1)–O(40) | 100.95(5) |
| O(15)–Fe(1)–O(40) | 100.02(6) |
| O(1)–Fe(1)–O(18) | 127.61(6) |
| O(15)–Fe(1)–O(18) | 117.19(6) |
| O(40)–Fe(1)–O(18) | 85.50(6) |
| O(1)–Fe(1)–N(8) | 88.05(5) |
| O(15)–Fe(1)–N(8) | 90.73(5) |
| O(40)–Fe(1)–N(8) | 161.90(6) |
| O(18)–Fe(1)–N(8) | 76.61(6) |

  

mon for $Fe^{III}$ with O,N-based ligation; octahedral coordination is by far the most common. The Fe–N and Fe–O bond lengths are consistent with a $d^5$ high-spin electron configuration of Fe(1), along with variable-temperature magnetic susceptibility measurements. The methanol molecule of crystallisation is hydrogen bonded to the carboxylate oxygen O(19) with an O(19)···HO(60) intermolecular distance of 2.74 Å. There is also a hydrogen bond between the methoxide oxygen O(40) and the triethylammonium cation with an O(40)···HN(50) contact of 2.65 Å. The bond lengths and angles in the cation $[(C_2H_5)_3NH]^+$ of **3** seem reasonable and do not warrant any special discussion.

### Molecular Structure of 4·2.5$CH_3CN$·$H_2O$

The asymmetric unit of **4** consists of two discrete crystallographically independent dinuclear monoanions and two triethylammonium monocations as well as two solvent molecules of crystallisation. The metrical parameters for the two crystallographically independent molecules in the anion observed for **4** are very similar and only one ORTEP diagram is shown (Figure 2); selected bond lengths and angles are summarised in Table 2. Both iron atoms, Fe(1) and Fe(2), are in distorted octahedral environments with $FeNO_5$ coordination spheres, although the nature of oxygen donor atoms is different. The two $FeNO_5$ coordination polyhedra share the edge that contains a phenoxo oxygen O(48) and a hydroxo group O(100), resulting in a four-membered $Fe_2O_2$ ring. The dihedral angle between the planes comprising Fe(1)–O(48)–Fe(2) and Fe(1)–O(100)–Fe(2) is 14.7°. The carboxylate oxygen O(4) and the phenolate oxygen O(28), being in mutually *trans* positions, form axial linkages for Fe(1), whereas N(1), phenolate O(18), bridging phenolate O(48) from the second $[L^2]^{3-}$ ligand and a hydroxo oxygen O(100) constitute the equatorial plane for Fe(1). On the other hand, the equatorial donor atoms for Fe(2) are four oxygen atoms: O(48), O(100),

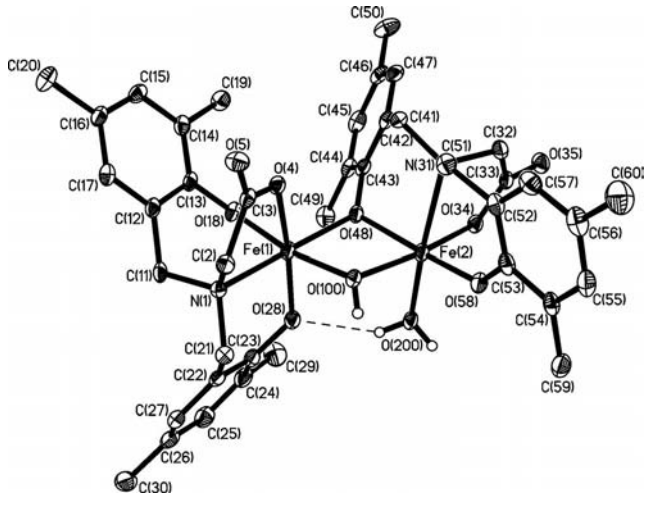


Figure 2. Molecular structure of **4** with ellipsoids drawn at the 40% probability level.

Table 2. Bond lengths [Å] and angles [°] for **4**·2.5$CH_3CN$·$H_2O$.[a]

| | |
|---|---|
| Fe(1)···Fe(2) | 3.118(1) |
| Fe(3)···Fe(4) | 3.127(1) |
| Fe(1)–O(18) | 1.920(2) |
| Fe(1)–O(28) | 1.935(2) |
| Fe(1)–O(48) | 2.003(2) |
| Fe(1)–O(100) | 2.030(2) |
| Fe(1)–O(4) | 2.093(2) |
| Fe(1)–N(1) | 2.192(2) |
| Fe(2)–O(58) | 1.875(2) |
| Fe(2)–O(100) | 1.968(2) |
| Fe(2)–O(34) | 2.038(2) |
| Fe(2)–O(48) | 2.038(2) |
| Fe(2)–O(200) | 2.053(2) |
| Fe(2)–N(31) | 2.208(3) |
| Fe(3)–O(78) | 1.922(2) |
| Fe(3)–O(88) | 1.935(2) |
| Fe(3)–O(108) | 2.000(2) |
| Fe(3)–O(300) | 2.043(2) |
| Fe(3)–O(64) | 2.065(2) |
| Fe(3)–N(61) | 2.194(2) |
| Fe(4)–O(118) | 1.872(2) |
| Fe(4)–O(300) | 1.967(2) |
| Fe(4)–O(94) | 2.043(2) |
| Fe(4)–O(400) | 2.044(2) |
| Fe(4)–O(108) | 2.052(2) |
| Fe(4)–N(91) | 2.189(2) |
| O(18)–Fe(1)–O(28) | 99.21(9) |
| O(18)–Fe(1)–O(48) | 97.84(8) |
| O(28)–Fe(1)–O(48) | 96.48(8) |
| O(18)–Fe(1)–O(100) | 168.89(9) |
| O(28)–Fe(1)–O(100) | 91.28(9) |
| O(48)–Fe(1)–O(100) | 77.21(8) |
| O(18)–Fe(1)–O(4) | 87.99(8) |
| O(28)–Fe(1)–O(4) | 166.29(9) |
| O(48)–Fe(1)–O(4) | 94.05(8) |
| O(100)–Fe(1)–O(4) | 82.51(8) |
| O(18)–Fe(1)–N(1) | 90.50(9) |
| O(28)–Fe(1)–N(1) | 90.49(9) |
| O(48)–Fe(1)–N(1) | 168.11(9) |
| O(100)–Fe(1)–N(1) | 93.07(9) |
| O(4)–Fe(1)–N(1) | 77.72(8) |
| O(58)–Fe(2)–O(100) | 95.08(9) |
| O(58)–Fe(2)–O(34) | 97.51(9) |
| O(100)–Fe(2)–O(34) | 167.12(9) |
| O(58)–Fe(2)–O(48) | 168.74(9) |
| O(100)–Fe(2)–O(48) | 77.82(8) |
| O(34)–Fe(2)–O(48) | 90.14(8) |
| O(58)–Fe(2)–O(200) | 100.70(9) |
| O(100)–Fe(2)–O(200) | 89.68(9) |
| O(34)–Fe(2)–O(200) | 85.32(9) |
| O(48)–Fe(2)–O(200) | 88.10(8) |
| O(58)–Fe(2)–N(31) | 87.34(9) |
| O(100)–Fe(2)–N(31) | 104.69(9) |
| O(34)–Fe(2)–N(31) | 78.69(9) |
| O(48)–Fe(2)–N(31) | 86.07(9) |
| O(200)–Fe(2)–N(31) | 162.95(9) |
| Fe(2)–O(100)–Fe(1) | 102.48(9) |
| Fe(1)–O(48)–Fe(2) | 100.95(9) |
| O(78)–Fe(3)–O(88) | 96.69(9) |
| O(78)–Fe(3)–O(108) | 99.44(9) |
| O(88)–Fe(3)–O(108) | 96.24(8) |
| O(78)–Fe(3)–O(300) | 172.70(9) |
| O(88)–Fe(3)–O(300) | 89.90(8) |
| O(108)–Fe(3)–O(300) | 76.63(8) |
| O(78)–Fe(3)–O(64) | 89.02(8) |
| O(88)–Fe(3)–O(64) | 166.85(8) |
| O(108)–Fe(3)–O(64) | 94.48(8) |
| O(300)–Fe(3)–O(64) | 85.19(8) |
| O(78)–Fe(3)–N(61) | 90.89(9) |

  

Table 2. *(continued)*

| | |
|---|---|
| O(88)–Fe(3)–N(61) | 89.86(9) |
| O(108)–Fe(3)–N(61) | 167.27(9) |
| O(300)–Fe(3)–N(61) | 92.27(9) |
| O(64)–Fe(3)–N(61) | 78.18(8) |
| O(118)–Fe(4)–O(300) | 96.60(9) |
| O(118)–Fe(4)–O(94) | 97.37(9) |
| O(300)–Fe(4)–O(94) | 165.75(9) |
| O(118)–Fe(4)–O(400) | 99.54(9) |
| O(300)–Fe(4)–O(400) | 90.83(8) |
| O(94)–Fe(4)–O(400) | 84.11(8) |
| O(118)–Fe(4)–O(108) | 170.25(8) |
| O(300)–Fe(4)–O(108) | 77.13(8) |
| O(94)–Fe(4)–O(108) | 89.37(8) |
| O(400)–Fe(4)–O(108) | 88.12(9) |
| O(118)–Fe(4)–N(91) | 87.43(9) |
| O(300)–Fe(4)–N(91) | 103.98(9) |
| O(94)–Fe(4)–N(91) | 79.46(9) |
| O(400)–Fe(4)–N(91) | 162.87(9) |
| O(108)–Fe(4)–N(91) | 86.88(9) |
| Fe(4)–O(300)–Fe(3) | 102.44(9) |
| Fe(3)–O(108)–Fe(4) | 101.01(9) |

[a] Symmetry transformations used to generate equivalent atoms.

carboxylate O(34) and phenolate O(58). Interestingly, O(200) of the coordinated water molecule and N(31) are in axial positions for Fe(2), thus indicating different coordination site-occupancy for two $[L^2]^{3-}$ anionic ligands; one $[L^2]^{3-}$ is ligated solely to Fe(1), whereas the second one shares a phenoxo oxygen O(48) between Fe(1) and Fe(2) resulting in the asymmetrically bridged diiron complex **4**. The largest deviation from the idealised 90° inter-bond angles is found within the five- and four-membered rings containing Fe(1) with the O(4)–Fe(1)–N(1) and O(48)–Fe(1)–O(100) at 77.72(8)° and 77.21(8)° angles, respectively. Similar deviations of inter-bond angles are also observed for Fe(2). It is noteworthy that the Fe(2)–O(48) bond length of 2.038(2) Å, involving a bridging phenolate oxygen, is, as expected, longer. This probably results in a comparatively short *trans*-positioned Fe(2)–O(58) bond length of 1.875(2) Å. The Fe–N and Fe–O bond lengths are consistent with the ferric ($d^5$ high spin) formulation for both the Fe(1) and Fe(2) centres. The $d^5$ high-spin electron configuration has also been confirmed by both magnetic susceptibility and Mössbauer (80 K, zero-field) measurements ($\delta_{Fe}$ = 0.52 mm s$^{-1}$; $\Delta E_Q$ = 1.15 mm s$^{-1}$). The Fe(1) ···Fe(2) separation of 3.118 Å is in the normal range.

It should be pointed out that the $H_3L^2$ ligand with methyl substituents results in the facile isolation of dinuclear complexes, such as **4**, whereas the sterically demanding ligand $H_3L^1$ containing *tert*-butyl derivatives with exactly the same donor atoms yields only mononuclear complexes, such as **1**–**3**. Our attempts to isolate dinuclear products with the ligand $H_3L^1$ are yet to be successful.

### X-ray Structure of 5

The structure of complex **5** consists of neutral, well-isolated dinuclear units of $[(L^3)_2Fe^{III}_2(\mu\text{-}OH)_2]$. Selected bond lengths and angles are listed in Table 3. An ORTEP view of the dimeric unit with a crystallographic twofold inversion symmetry is shown in Figure 3. The structure consists of an edge-shared bioctahedron for the diiron(III) core. The asymmetric unit contains half of the dimer and consequently the geometries of the two iron centres are identical, with ligation provided by the O(30) and O(30)* atoms of the bridging hydroxy ligands, two phenolate oxygen atoms O(1) and O(17), one amine nitrogen N(9) and one pyridine nitrogen N(24) belonging to the terminal ligand $[L^3]^{2-}$, resulting in a distorted octahedral arrangement for each iron centre. The symmetrically dibridged four-membered $Fe_2(\mu\text{-}OH)_2$ ring is planar. The pyridine nitrogen N(24) is in the *trans* position

Table 3. Bond lengths [Å] and angles [°] for complex **5**.[a]

| | |
|---|---|
| Fe(1)–O(1) | 1.9033(8) |
| Fe(1)–O(17) | 1.9350(7) |
| Fe(1)–O(30) | 1.9846(8) |
| Fe(1)–O(30)#1 | 2.0853(8) |
| Fe(1)–N(24) | 2.2053(9) |
| Fe(1)–N(9) | 2.2265(9) |
| O(1)–Fe(1)–O(17) | 96.47(3) |
| O(1)–Fe(1)–O(30) | 99.53(3) |
| O(17)–Fe(1)–O(30) | 99.33(3) |
| O(1)–Fe(1)–O(30)#1 | 91.22(3) |
| O(17)–Fe(1)–O(30)#1 | 172.30(3) |
| O(30)–Fe(1)–O(30)#1 | 79.59(3) |
| O(1)–Fe(1)–N(24) | 166.04(3) |
| O(17)–Fe(1)–N(24) | 89.12(3) |
| O(30)–Fe(1)–N(24) | 92.12(3) |
| O(30)#1–Fe(1)–N(24) | 83.32(3) |
| O(1)–Fe(1)–N(9) | 91.40(3) |
| O(17)–Fe(1)–N(9) | 88.31(3) |
| O(30)–Fe(1)–N(9) | 165.81(3) |
| O(30)#1–Fe(1)–N(9) | 91.24(3) |
| N(24)–Fe(1)–N(9) | 75.94(3) |
| Fe(1)–O(30)–Fe(1)#1 | 100.41(3) |

[a] Symmetry transformations used to generate equivalent atoms: #1 $-x + 1, -y, -z + 1$.

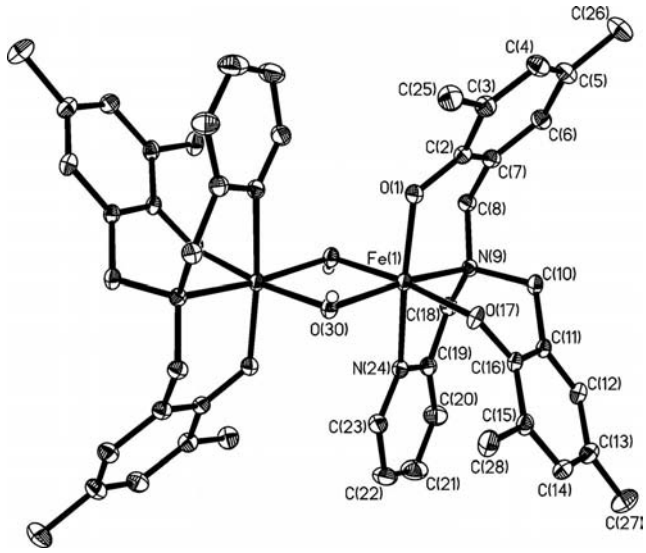


Figure 3. Molecular structure of **5** with ellipsoids drawn at the 50% probability level.

  

to the phenolate O(1) yielding an O(1)–Fe(1)–N(24) angle of 166.01(4)°. The Fe–O and Fe–N bond lengths are in conformation with the high-spin $d^5$ electron configuration for the ferric centres in **5**, which corroborates with the magnetic measurements. The Fe···Fe separation of 3.128 Å is comparable with those reported for other dihydroxo-bridged diferric(III) complexes.

### Molecular Structure of 6

Figure 4 displays a perspective view of the discrete neutral dinuclear units $[(L^3)_2Fe^{III}_2(\mu\text{-}OCH_3)(\mu\text{-}OOCCH_3)]$ and their atom labelling scheme. Selected bond lengths and angles are listed in Table 4. The structural data concerning the $[L^3]^{2-}$-containing parts of the complex are in good agreement with those of previous studies[6e,7c] using the same ligand and do not warrant any detailed description. The Fe(1) and Fe(2) iron atoms are asymmetrically bridged by one methoxy O(60) and one *syn*,*syn* $\eta^1{:}\eta^1{:}\mu_2$ acetate ligand [O(70) and O(72)]. Each iron centre is in a distorted octahedral environment with an $FeN_2O_4$ coordination sphere. The bond lengths Fe(1)–O(70) 2.067(5) Å and Fe(2)–O(72) 2.078(5) Å, involving the acetate bridging, are in agreement with similar (μ-acetato)diiron(III) complexes.[14] The bridging methoxy O(60) constitutes a nearly linear array with bond angles N(9)–Fe(1)–O(60) of 175.8(2)° and N(39)–Fe(2)–O(60) of 175.9(2)°. The pyridine nitrogens, N(24) and N(54), are *trans* disposed through the iron centres to phenolate oxygens with bond angles N(24)–Fe(1)–O(17) of 164.8(2)° and N(54)–Fe(2)–O(31) of 164.0(2)°. The Fe–O and Fe–N bond lengths are consistent with a $d^5$ high-spin electron configuration for both $Fe^{III}$ centres with amine nitrogen and phenolate oxygen-donor ligands. The Fe···Fe separation of 3.549 Å is slightly longer than that for **5** and similar to other complexes.

Table 4. Bond lengths [Å] and angles [°] for **6**.

| | |
|---|---|
| Fe(1)–O(17) | 1.900(6) |
| Fe(1)–O(1) | 1.945(5) |
| Fe(1)–O(60) | 1.984(5) |
| Fe(1)–O(70) | 2.067(5) |
| Fe(1)–N(24) | 2.218(7) |
| Fe(1)–N(9) | 2.221(6) |
| Fe(2)–O(31) | 1.899(6) |
| Fe(2)–O(47) | 1.960(5) |
| Fe(2)–O(60) | 1.963(5) |
| Fe(2)–O(72) | 2.078(5) |
| Fe(2)–N(54) | 2.177(7) |
| Fe(2)–N(39) | 2.230(6) |
| O(17)–Fe(1)–O(1) | 102.0(2) |
| O(17)–Fe(1)–O(60) | 94.5(2) |
| O(1)–Fe(1)–O(60) | 94.0(2) |
| O(17)–Fe(1)–O(70) | 93.8(2) |
| O(1)–Fe(1)–O(70) | 162.6(2) |
| O(60)–Fe(1)–O(70) | 92.0(2) |
| O(17)–Fe(1)–N(24) | 164.8(2) |
| O(1)–Fe(1)–N(24) | 83.9(2) |
| O(60)–Fe(1)–N(24) | 99.1(2) |
| O(70)–Fe(1)–N(24) | 79.1(2) |
| O(17)–Fe(1)–N(9) | 88.2(2) |
| O(1)–Fe(1)–N(9) | 88.5(2) |
| O(60)–Fe(1)–N(9) | 175.8(2) |
| O(70)–Fe(1)–N(9) | 84.7(2) |
| N(24)–Fe(1)–N(9) | 77.8(3) |
| O(31)–Fe(2)–O(47) | 103.1(2) |
| O(31)–Fe(2)–O(60) | 93.6(2) |
| O(47)–Fe(2)–O(60) | 94.4(2) |
| O(31)–Fe(2)–O(72) | 90.6(2) |
| O(47)–Fe(2)–O(72) | 164.2(2) |
| O(60)–Fe(2)–O(72) | 92.5(2) |
| O(31)–Fe(2)–N(54) | 164.0(2) |
| O(47)–Fe(2)–N(54) | 85.5(2) |
| O(60)–Fe(2)–N(54) | 99.2(2) |
| O(72)–Fe(2)–N(54) | 79.4(2) |
| O(31)–Fe(2)–N(39) | 89.5(2) |
| O(47)–Fe(2)–N(39) | 87.5(2) |
| O(60)–Fe(2)–N(39) | 175.9(2) |
| O(72)–Fe(2)–N(39) | 84.8(2) |
| N(54)–Fe(2)–N(39) | 77.3(2) |
| Fe(2)–O(60)–Fe(1) | 128.1(3) |
| Fe(1)–O(70)–C(71) | 126.2(5) |
| Fe(2)–O(72)–C(71) | 127.9(5) |

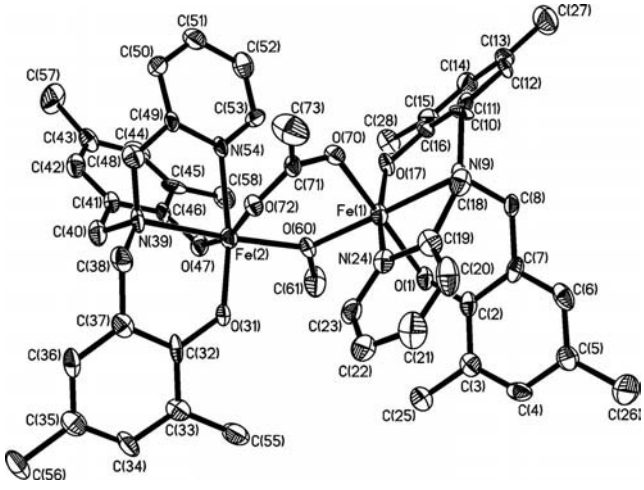


Figure 4. ORTEP plot of **6** with ellipsoids drawn at the 50% probability level.

### Crystal Structures of $7{\cdot}2CH_3CN$ and $8{\cdot}CH_3OH$

As complexes **7** and **8** contain the same tridentate $[L^4]^{2-}$ anion with the same substituents, *para*-disposed methyl and *ortho*-substituted *tert*-butyl to phenol groups, the X-ray structures are described under the same heading.

Single crystals of deep red-brown dinuclear neutral molecules $[(L^4)_2Fe^{III}_2(\mu\text{-}OH)_2]{\cdot}2CH_3CN$ (**7**) were obtained from an acetonitrile solution by slow evaporation. The asymmetric unit contains half of the dimer and a solvent molecule of crystallisation. The molecular geometry and the atom labelling scheme for the molecule in **7** are shown in Figure 5. Bond lengths and angles are selectively listed in Table 5. The two iron centres are bridged by two hydroxo groups, which are weakly hydrogen bonded to the N(40) and N(40)* atoms [O(1)···N(40) 2.99 Å] of the solvent acetonitrile. The five-fold coordination of the iron centres is completed by the dianionic ligand $[L^4]^{2-}$ through the amine nitrogen N(19) and two

  

phenolate oxygens O(27) and O(1); this generates two $FeNO_4$ coordination spheres. The geometry of the iron centres is best described as a trigonal bipyramid (trigonality index $\tau$ = 0.839) with three oxygen atoms, namely, the bridging hydroxo O(1) and the phenoxo oxygens O(11) and O(27), forming the equatorial plane; the axial ligation is fulfilled by N(19) and O(27) [N(19)–Fe(1)–O(1)* 171.69(4)°]. The structures of **7** and **5** primarily differ from one another in the coordination number of the iron centre, five for **7** and six for **5**, which can be attributed to the denticity of the corresponding ancillary ligands. The bond lengths for the five-coordinate iron centres in **7** are significantly shorter than those for the six-coordinate iron centres in **5**. The Fe–N and Fe–O bond lengths are consistent with a $d^5$ high-spin electron configuration of the iron in both cases, which is also in agreement with magnetic susceptibility measurements. The Fe···Fe separation of 3.066 Å in **7** is very similar to that for **5** and other hydroxo-bridged diferric(III) complexes.

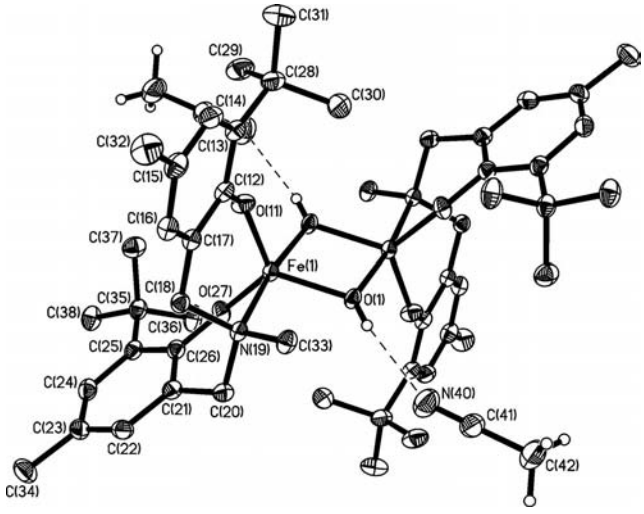


Figure 5. ORTEP diagram of **7**·2$CH_3CN$ with ellipsoids drawn at the 50% probability level.

Table 5. Bond lengths [Å] and angles [°] for **7**·2$CH_3CN$.[a]

| | |
|---|---|
| Fe(1)–O(27) | 1.8570(11) |
| Fe(1)–O(11) | 1.8605(11) |
| Fe(1)–O(1) | 1.9305(10) |
| Fe(1)–O(1)#1 | 2.0037(11) |
| Fe(1)–N(19) | 2.1942(12) |
| O(1)–Fe(1)#1 | 2.0036(11) |
| O(27)–Fe(1)–O(11) | 121.03(5) |
| O(27)–Fe(1)–O(1) | 117.54(5) |
| O(11)–Fe(1)–O(1) | 121.40(5) |
| O(27)–Fe(1)–O(1)#1 | 96.15(5) |
| O(11)–Fe(1)–O(1)#1 | 94.41(5) |
| O(1)–Fe(1)–O(1)#1 | 77.64(5) |
| O(27)–Fe(1)–N(19) | 89.25(5) |
| O(11)–Fe(1)–N(19) | 88.14(5) |
| O(1)–Fe(1)–N(19) | 94.31(5) |
| O(1)#1–Fe(1)–N(19) | 171.72(4) |
| Fe(1)–O(1)–Fe(1)#1 | 102.36(5) |

[a] Symmetry transformations used to generate equivalent atoms: #1 $-x, -y, -z$.

In an attempt to prepare a bis(μ-methoxo)diiron(III) complex, **7** was recrystallised from a methanolic solution in the presence of a relatively strong base [$n$$Bu_4N$]$OCH_3$. The asymmetrically bridged (μ-hydroxo) (μ-methoxo) complex **8**·$CH_3OH$ was isolated as deep brown crystals. A view of the structure is shown in Figure 6 and selected bond lengths and angles are listed in Table 6. The structure analysis of **8** shows, in contrast to **7**, the presence of a five- and a six-coordinate iron centre [Fe(2) and Fe(1), respectively]. Such dissimilar coordination numbers for the two iron centres in a diferric(III) complex has been observed for another dimethyl-substituted aminebis(phenolate) ligand.[6a]

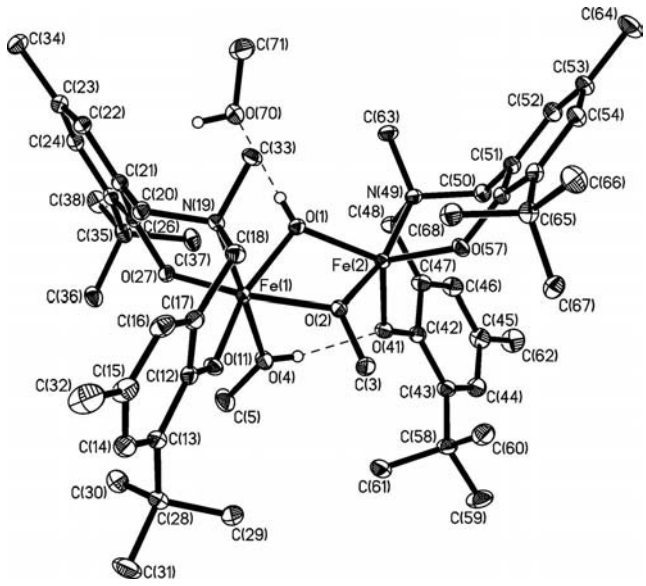


Figure 6. ORTEP diagram of **8** with ellipsoids drawn at the 40% probability level.

The Fe(1) centre is in a distorted octahedral environment with an $FeNO_5$ coordination sphere, whereas Fe(2) is in a distorted trigonal pyramidal $FeNO_4$ environment. Two oxygen atoms, a hydroxo O(1) and a methoxy O(2) act as bridging ligands between the Fe(1) and Fe(2) centres. Each metal ion is terminally coordinated to the dianionic ligand $[L^4]^{2-}$, thus rendering them five-coordinate; a methanol molecule O(4) completes the sixth coordination site for Fe(1). The severe distortion of Fe(2) from a regular polyhedron (the trigonality index $\tau$ = 0.493) is shown by the equatorial angles O(1)–Fe(2)–O(57) 138.37(6)°, O(57)–Fe(2)–O(41) 113.87(6)° and O(41)–Fe(2)–O(1) 107.71(6)°. The bridging angles Fe(2)–O(1)–Fe(1) 102.79(6)° and Fe(2)–O(2)–Fe(1) 103.04(6)° are very similar. Hydrogen bonds exist between the free methanol and bridging O(1) [O(70)H···O(1) 2.94 Å], and between coordinated methanol and phenolate O(41) [O(4)H···O(41) 2.72 Å], as exhibited by the dotted lines in Figure 6. For Fe(1), bridging oxygens O(1) and O(2), and phenolates O(11) and O(27) constitute the equatorial plane, whereas the amine N(19) and the methanol O(4) are in the axial sites. The Fe(1)···Fe(2) separation of 3.128 Å falls in the range of reported values. The dihedral angle between the planes comprising Fe(1)–O(1)–Fe(2) and Fe(1)–O(2)–Fe(2) is 28.4°.

  

Table 6. Bond lengths [Å] and angles [°] for **8**·$CH_3OH$.

| | |
|---|---|
| Fe(1)–O(11) | 1.8893(13) |
| Fe(1)–O(27) | 1.9098(13) |
| Fe(1)–O(2) | 2.0220(13) |
| Fe(1)–O(1) | 2.0678(13) |
| Fe(1)–O(4) | 2.1416(14) |
| Fe(1)–N(19) | 2.1971(15) |
| Fe(2)–O(57) | 1.8518(14) |
| Fe(2)–O(41) | 1.9089(13) |
| Fe(2)–O(1) | 1.9329(13) |
| Fe(2)–O(2) | 1.9731(13) |
| Fe(2)–N(49) | 2.2076(15) |
| O(11)–Fe(1)–O(27) | 101.31(6) |
| O(11)–Fe(1)–O(2) | 92.89(5) |
| O(27)–Fe(1)–O(2) | 163.81(6) |
| O(11)–Fe(1)–O(1) | 165.19(6) |
| O(27)–Fe(1)–O(1) | 93.45(5) |
| O(2)–Fe(1)–O(1) | 72.32(5) |
| O(11)–Fe(1)–O(4) | 90.92(6) |
| O(27)–Fe(1)–O(4) | 87.50(6) |
| O(2)–Fe(1)–O(4) | 84.51(6) |
| O(1)–Fe(1)–O(4) | 88.49(5) |
| O(11)–Fe(1)–N(19) | 89.24(6) |
| O(27)–Fe(1)–N(19) | 90.25(5) |
| O(2)–Fe(1)–N(19) | 97.74(6) |
| O(1)–Fe(1)–N(19) | 91.93(5) |
| O(4)–Fe(1)–N(19) | 177.73(6) |
| O(57)–Fe(2)–O(41) | 113.81(6) |
| O(57)–Fe(2)–O(1) | 138.37(6) |
| O(41)–Fe(2)–O(1) | 107.72(6) |
| O(57)–Fe(2)–O(2) | 95.87(6) |
| O(41)–Fe(2)–O(2) | 96.44(6) |
| O(1)–Fe(2)–O(2) | 76.32(5) |
| O(57)–Fe(2)–N(49) | 88.81(6) |
| O(41)–Fe(2)–N(49) | 91.76(6) |
| O(1)–Fe(2)–N(49) | 92.82(6) |
| O(2)–Fe(2)–N(49) | 167.96(6) |
| Fe(2)–O(1)–Fe(1) | 102.79(6) |
| Fe(2)–O(2)–Fe(1) | 103.04(6) |

## Magnetic Susceptibility Measurements

Magnetic susceptibility data for polycrystalline samples of complexes **1**–**8** were collected in the temperature range 2–290 K in an applied magnetic field of 1 T. The magnetic properties of mononuclear complexes **1**–**3** exhibit, above 20 K, the essentially temperature-independent magnetic moment values $\mu_{eff} = 5.90 \pm 0.01\ \mu_B$, and thus clearly contain high-spin $d^5$ ions, that is high spin $Fe^{III}$.

The magnetic behaviour of complexes **4**–**8** is characteristic of antiferromagnetically coupled dinuclear complexes. For example, at 290 K the $\mu_{eff}$ value of 6.33 $\mu_B$ ($\chi_M{\cdot}T$ = 5.002 $cm^3\,K\,mol^{-1}$) for **6** or of 8.19 $\mu_B$ ($\chi_M{\cdot}T$ = 8.379 $cm^3\,K\,mol^{-1}$) for **7** decreases monotonically with decreasing temperature until it reaches a value of 0.30 $\mu_B$ ($\chi_M{\cdot}T$ = 0.01169 $cm^3\,K\,mol^{-1}$) for **6** or 1.22 $\mu_B$ ($\chi_M{\cdot}T$ = 0.1862 $cm^3\,K\,mol^{-1}$) for **7** at 2 K (Figure 7). This is a clear indication of exchange coupling between two paramagnetic high-spin $Fe^{III}$ centres ($S_{Fe}$ = 5/2) with a resulting $S_t$ = 0 ground state. We used the Heisenberg–Dirac–van Vleck spin-Hamiltonian in the form $\hat{H} = -2J\hat{S}_1{\cdot}\hat{S}_2$ for an isotropic exchange coupling between two spins $S_1$ and $S_2$. The solid lines in Figure 7 represent the best fits[15] with the following parameters: $J$ = –14.1 $cm^{-1}$, $g_1 = g_2$ = 2.00 (fixed) and monomeric paramagnetic impurity (S = 5/2) PI = 0.03% for **6** and $J$ = –2.1 $cm^{-1}$, $g_1 = g_2$ = 2.00 (fixed) for **7**. Similar weak antiferromagnetic exchange coupling constants have been evaluated for other complexes and are listed in Table 7. As the evaluation of coupling constants for such dinuclear com-

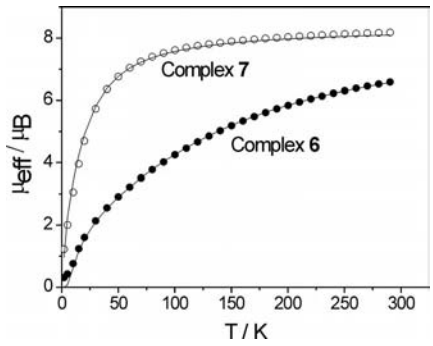


Figure 7. Plots of $\mu_{eff}$ versus $T$ for complexes **6** and **7**. The solid lines represent the simulation of the experimental data to the theoretical equation (see text).

Table 7. Selected structural data and exchange coupling constants ($\hat{H} = -2J\hat{S}_1{\cdot}\hat{S}_2$) for reported diferric(III) complexes doubly bridged by two different ligands and for complexes **4**–**8**.

| Complexes[a] with (μ-OX)(μ-OY) groups[b] | av. Fe–O(bridge) [Å] | Fe–O–Fe [°] | $J$ [$cm^{-1}$] | Ref. |
|---|---|---|---|---|
| **4** (OH)(OPh) | 2.01 | 101.7 | –7.0 | this work |
| **5** (OH)(OH) | 2.034 | 100.5 | –4.1 | this work |
| **6** (OMe)(OAc) | 2.023 | 128.1 | –14.1 | this work |
| **7** (OH)(OH)[c] | 1.966 | 102.5 | –2.1 | this work |
| **8** (OH)(OMe)[d] | 1.999 | 102.9 | –6.0 | this work |
| **9** (OH)(OMe)[d] | 1.999 | 102.4 | –5.84 | [6f] |
| **10** (OMe)(OMe) | 2.016 | 104.7 | –26.8 | [16] |
| **11** (OMe)(OMe) | 1.997 | 104.3 | –28.6 | [16] |
| **12** (OMe)(OMe) | 1.987 | 102.0 | –7.7 | [17] |
| **13** (OMe)(OMe) | 1.974 | 103.7 | –9.5 | [17] |
| **14** (OR)(OOCR) | 1.971 | 130.0 | –14.4 | [14a] |
| **15** (OR)(OOCR) | 1.986 | 129.3 | –14.0 | [18] |
| **16** (OH)(OAc) | 1.990 | 126.4 | –14.3 | [19] |
| **17** (OH)(OPh) | 1.985 | 104.4 | –12.0 | [20] |
| **18** (OMe)(OR) | 2.010 | 102.8 | –10.6 | [21] |
| **19** (OMe)(OAc) | 2.045 | 101.0(OAc), 108.7(OMe) | –8.3 | [22] |
| **20** (OH)(OPh) | 2.018 | 103.5 | –7.4 | [23] |
| **21** (OMe)(OPh) | 2.013 | 102.5 | –8.0 | [24] |
| **22** (OR)(OR) | 1.972 | 104.1 | –17.0 | [25] |
| **23** (OR)(OR) | 2.024 | 101.1 | –2.2 | [26] |
| **24** (OPh)(OPh)[c] | 2.006 | 105.7 | –10.4 | [27] |
| **25** (OR)(OR)[c] | 1.967 | 104.5 | –15.8 | [28] |
| **26** (OPh)(OPh) | 2.044 | 97.1 | +1.2 | [29] |
| **27** (OPh)(OPh) | 2.043 | 108.9 | –12.7 | [30] |
| **28** (OPh)(OPh)[d] | 2.054 | 104.9 | –7.4 | [6a] |

[a] Only the bridging ligands are denoted. The terminal ligands and the diiron(III) centres have been omitted for clarity. [b] OPh = phenoxide; OMe = methoxide, OR = alkoxide, OAc = acetate; monoatomic O-bridging of OAc in **19**. [c] Both iron(III)-centres are five coordinate. [d] Only one of the two iron centres is five coordinate.

  

plexes is now a matter of routine work, we refrain from describing them in detail. We have chosen to display the results for complexes **6** and **7** (Figure 7) as they exhibit the strongest and the weakest coupling of the present series. Additionally, complex **7** represents a rare case of exchange-coupled five-coordinate ferric(III) centres.

It has been reported[34b] that different analysis of the same susceptibility data can lead to varying $J$ values, when the $g$ value is allowed to float for a ferric centre. In our case, for example, the susceptibility data for complex **5** could be simulated with the same good quality when the $g$ value is floated. Thus, the $J$ values vary between –3.15 with $g$ = 1.883 and –3.66 $cm^{-1}$ with $g$ = 1.95. Because of the spherical electron distribution of high-spin $d^5$ ions, the $g$ value is expected to be equal to 2.00 in accordance with the $^6A_1$ ground state. Hence, we have kept a fixed $g$ = 2.00 value for complexes **4**–**8**.

Table 7, which includes the diferric(III) complexes of the present series (**4**–**8**), was assembled with consideration of the following points: (i) all structurally characterised asymmetrically doubly bridged diiron(III) complexes are included; (ii) as the non-linear triatomic bridging groups, such as tetraoxometalates,[31] are very weak exchange couplers the diiron(III) complexes bridged by ion such as chromate, molybdate, and sulfate have been excluded; selected triatomic bridging through acetate and other carboxylato groups, which are also very weak transmitters of spin coupling are listed for the necessity of comparison with the only known (μ-methoxy)(μ-acetato)diiron complex **6**; (iii) although the symmetrically monoatomic(III) dibridged diferric complexes are abundant,[32] only a few of them have been listed to indicate the range of weak ferromagnetism (**26**) to moderate weak antiferromagnetism (**11**).

Due to Fe···Fe distances longer than 3 Å in all complexes listed in Table 7 any correlation between this structural feature and the exchange coupling constant $J$ can be safely excluded.[33] The presence of ten magnetic orbitals, originating from five singly occupied d-orbitals per high-spin ferric ion and resulting in a large number of crossed- and direct-exchange pathways makes any clear-cut analysis of the magnetic behaviour for diferric(III) complexes, particularly with weak exchange coupling, very difficult. Accordingly, none of the proposed magnetostructural correlations[32,34] relating to the magnitude of the exchange coupling to either the iron-bridging oxygen bond length or the bridging Fe–O–Fe angle can satisfactorily rationalise the weak-coupled systems listed in Table 7. Irrespective of the planarity of the bridging $Fe_2O_2$ unit, the Fe–O–Fe bridge angle and the Fe–O(bridge) bond length have their independent contributory roles to the overall exchange coupling $J$, in which one structural feature can outweigh the other. For example, in complex **6**, *syn*,*syn* $\eta^1$:$\eta^1$-acetato bridging yields a large Fe–OMe–Fe bridging angle of 128.1° resulting in the strongest coupling for the present series. Similarly, the strength of exchange coupling increases with bridging angle for **12**–**14**, in spite of very similar Fe–O bond lengths of ≈1.98 Å. Indeed, a linear dependence of $J$ on the bridging angle for similar complexes has been reported.[17] Additionally, complexes **8** and **9**, with nearly identical above-mentioned structural parameters, exhibit, as expected, very similar spin coupling. The weakest coupling in the series is observed for complex **7**, containing a bis(μ-hydroxo) bridge, as the Fe–O–Fe angle is small in conjunction with the expected Fe–O bond length (1.966 Å) for five-fold coordination of $Fe^{III}$. On the contrary, complex **25** with five-coordinate bis(μ-alkoxo) diferric(III) centres results in a $J$ value of –15.8 $cm^{-1}$ in spite of the same Fe–O bond length (1.967 Å), presumably due to the larger bridging angle (104.5°). The ferromagnetic interaction observed only for complex **26**, a bis(μ-phenoxo)diiron(III) compound, has been attributed[29] to the smallest Fe–O–Fe angle (97°). In the above discussion, we have not considered the effect of the groups –H, –R, –Me and –Ph on the electron density of the bridging oxygen atom. Considering the I-effects, it is expected that the methoxo-bridged compounds should show strongest antiferromagnetic interactions, which is indeed the case as exemplified by complexes **9** and **10**. No striking correlation is established, however, between only one structural parameter and the magnitude of the exchange coupling.

The strength of exchange coupling is weaker in the five-coordinate than the six-coordinate $Fe^{III}$ species, as exemplified by the $J$ values for complexes **5** and **7**, in spite of the fact that the average Fe–O bond length is shorter and the Fe–O–Fe angle larger in five-coordinate **7** than those in six-coordinate **5**.

It is interesting to note that complexes **6**, **14**, **15** and **16** (Table 7) exhibit very similar exchange couplings ($J$ ≈ –14 $cm^{-1}$), although the Fe–O bond lengths vary in the range 1.971–2.023 Å in conjunction with the comparatively larger Fe–O–Fe angles (126–130°).

## Conclusion

To conclude, the following points of this study deserve particular attention.

As an obvious progression of our earlier reports[6] on ligating properties of amine-bis(phenolate) ligands with [O,N,O] donor atoms, we have studied dimethyl- versus di-*tert*-butyl-substituted phenol-based ligands ($H_3L^1$ versus $H_3L^2$) and observed a noteworthy effect of *tert*-butyl groups on the nuclearity of the ferric(III) compounds. Only mononuclear complexes **1**–**3** have been isolated with $H_3L^1$ in contrast to the diferric(III) complex **4** with the dimethyl congener $H_3L^2$.

Emphasis has been given to structural and magnetic studies of the asymmetrically dibridged diferric(III) complexes **4**–**8**, whose exchange coupling properties have been compared to those of similar compounds from the literature to judge the spin exchange ability of the different groups, such as –OH, –OMe, –OR and –OPh. A comparison between five- and six-coordinate diferric(III) centres, regarding exchange coupling, is reported. It appears that for the diferric(III) series **4**–**8**, the structural feature, the bridging Fe–O–Fe angle, is a major factor in determining the strength of the exchange interaction. Inspection of similar compounds from the literature also shows a dependence of $J$ on the Fe–O(bridging) bond length. Thus, no definitive magneto-structural conclusion based only on a single structural parameter of the re-

  

ported weakly-coupled diiron(III) complexes has been obtained.

## Experimental Section

**Materials and Physical Measurements:** Reagent or analytical grade materials were obtained from commercial suppliers and used without further purification. Elemental analyses (C, H, N, and metal) were performed by the Microanalytical Laboratory, Mülheim, Germany. FT-IR spectra of the samples in KBr disks were recorded with a Perkin–Elmer 2000 FT-IR instrument. Magnetic susceptibilities of powdered samples were recorded with a SQUID magnetometer in the temperature range 2–290 K with an applied field of 1 T. Experimental susceptibility data were corrected for the underlying diamagnetism using Pascal's constants. Mass spectra were recorded with either a Finnigan MAT 8200 (electron ionisation) or a MAT 95 (electrospray ionisation, ESI-MS) instrument. A Bruker DRX 400 instrument was used for NMR spectroscopy.

**Syntheses of Ligands:**[4,5a,7] The ligands [*N*,*N*-bis(3,5-di-*tert*-butyl)-2-hydroxybenzyl]aminoacetic acid ($H_3L^1$), (*N*,*N*-bis[2-hydroxy-3,5-dimethylbenzyl]aminoacetic acid) ($H_3L^2$), [*N*,*N*-bis(2-hydroxy-3,5-dimethylbenzyl)]-*N*-(2-pyridylmethyl)amine ($H_2L^3$) and [methylamino-*N*,*N*-bis(6-*tert*-butyl-4-methyl-2-methylenephenol)] ($H_2L^4$) were prepared by the one-pot Mannich condensation reaction of phenol with the appropriate substituents (0.1 mol), formaldehyde 37% (0.1 mol) and glycine (0.05 mol) for $H_3L^1$ and $H_3L^2$, 2-(aminomethyl)pyridine (0.05 mol) for $H_2L^3$ or methylamine (0.05 mol) for $H_2L^4$ in dry methanol as solvent. The reaction mixture was stirred overnight and then refluxed for 3 h. On cooling, a white solid was obtained, which was filtered off, and washed with water and methanol.

The purity of the ligands was checked by liquid chromatography.

**$H_3L^1$:** Yield 51%. $^1$H NMR ($CDCl_3$, 400 MHz): $\delta$ = 1.25–1.40 (36 H), 1.99 (s, 4 H), 3.45 (s, 2 H), 3.77, 3.79 (d, 4 H), 6.88, 6.89 (d, 4 H) ppm. IR (KBr ): $\tilde{\nu}$ = 2962 (m), 1705 (s), 1636 (s), 1482 (s), 1361 (m), 1292 (m), 1222 (s) cm$^{-1}$. EI-MS: *m*/*z* (%) = 511 (18) [$M^+$], 293 (50) [M – $C_{15}H_{23}O$], 219 (28) [$C_{15}H_{23}O$], 203 (100) [$C_{15}H_{21}$].

**$H_3L^2$:** Yield 68%; m.p. 199–201 °C. Nearly insoluble for $^1$H NMR spectroscopy. IR (KBr ): $\tilde{\nu}$ = 3456 (m), 3005 (m), 1641 (s), 1491 (s), 1439 (m), 1401 (m), 1386 (s), 1324 (m), 1199 (s), 1159 (m) cm$^{-1}$. EI-MS: *m*/*z* (%) = 343 (38) [$M^+$], 298 (6) [M – COOH], 209 (67) [M – $C_9H_{11}O$], 135 (100) [$C_9H_{11}O$].

**$H_2L^3$:** Yield 46%; m.p. 122–124 °C. $^1$H NMR (400 MHz, $CDCl_3$): $\delta$ = 2.17–2.25 (12 H), 3.74, 3.82 (6 H), 6.69 (2 H), 6.85 (2 H), 7.10 (1 H), 7.24–7.27 (1 H), 7.66–7.71 (1 H), 8.68–8.69 (1 H) ppm. IR (KBr): $\tilde{\nu}$ = 3125 (m), 3006 (m), 2964 (m), 2849 (m), 2727 (m), 1597 (s), 1571 (m), 1498 (vs), 1431 (s), 1371 (s), 1290 (s), 1223 (vs), 1158 (s), 1028 (s), 1003 (s), 973 (s), 864 (s), 851 (s), 760 (s), 737 (s) cm$^{-1}$. EI-MS: *m*/*z* (%) = 376 (19) [$M^+$], 284 (56) [M – $C_5H_4N(CH_2)$], 241 (100) [M – $C_6H_2(CH_3)_2(CH_2)(OH)$].

**$H_2L^4$:** Yield 18%; m.p. 99–102 °C. IR (KBr ): $\tilde{\nu}$ = 3629 (sharp s), 3443 (br. s), 2955, 2918, 2864 (s), 1609 (m), 1481, 1468, 1445 (s), 1388 (m), 1357 (m), 1301 (m), 1280 (m), 1237 (s), 1180 (m), 1126 (m), 1025 (m), 977 (m), 863 (s), 843 (s), 798 (m), 772 (m), 757 (s) cm$^{-1}$. EI-MS: *m*/*z* (%) = 383 (85) [$M^+$], 207 (100) [M – $C_6H_2(CH_3)(C_4H_9)(CH_2)$-OH], 177 [$C_6H_2(CH_3)(C_4H_9)(CH_2)(OH)$].

**Preparation of Complexes**

**[($L^1$)$Fe^{III}(H_2O)$] (1):** $FeCl_2{\cdot}4H_2O$ (0.19 g, 1 mmol) was added to a degassed solution of $CH_3OH$ (50 mL) containing $H_3L^1$ (0.51 g, 1 mmol). Upon addition of $Et_3N$ (0.4 mL) the colour of the solution turned red-brown. The solution was refluxed in air for 1 h and filtered to remove any solid particles. The deep brown microcrystalline solid that separated after cooling was recrystallised from methanol; yield 110 mg (20%). $C_{32}H_{48}FeNO_5$ (582.59): calcd. C 65.97, H 8.31, N 2.40, Fe 9.59; found C 66.4, H 8.3, N 2.5, Fe 9.8. IR (KBr): $\tilde{\nu}$ = 2958, 2868, 2678, 1627, 1470, 1439, 1413, 1361, 1305, 1263, 1240, 1204, 1171, 1130, 877, 841, 752, 613 cm$^{-1}$. ESI-MS (positive mode, $CH_3CN$ solution): *m*/*z* (%) = 582 [$M^+$]. UV/Vis [$CH_3OH$]: $\lambda_{max}$, nm ($\varepsilon$, $M^{-1}cm^{-1}$): 282 ($21.7\times10^3$), 381 ($10.1\times10^3$), 510 ($6.0\times10^3$).

**[($L^1$)$Fe^{III}(C_2H_5OH)$] (2):** Complex **2** was obtained from **1** after recrystallisation from an ethanolic solution. $C_{34}H_{52}FeNO_5$ (610.64): calcd. C 66.88, H 8.58, N 2.29, Fe 9.15; found C 67.0, H 8.6, N 2.2, Fe 9.1.

**[($L^1$)$Fe^{III}(OCH_3)$][$Et_3NH$] (3):** The same protocol used for **1** was used complex **3** but an excess of $Et_3N$ (4.0 mL) was added. Deep-brown crystals were obtained from a methanol solution for the X-ray structure determination; yield 0.35 g (≈50%). $C_{39}H_{65}FeN_2O_5$ (697.81): calcd. C 67.13, H 9.39, N 4.02, Fe 8.00; found C 67.0, H 9.3, N 4.1, Fe 7.9. IR (KBr): $\tilde{\nu}$ = 2958, 2905, 2869, 1655, 1474, 1438, 1413, 1387, 1361, 1305, 1267, 1240, 1204, 1170, 1131, 1109, 877, 863, 840, 810, 751, 613 cm$^{-1}$. ESI-MS (negative mode, $CH_3OH$ solution): *m*/*z* = 595 [M – $Et_3NH$].

**[$Et_3NH$][($L^2$)$_2Fe^{III}_2$(μ-OH)($OH_2$)] (4):** A solution of the ligand $H_3L^2$ (0.34 g, 1 mmol) and $Et_3N$ (0.4 mL) in methanol (50 mL) was degassed for 15 min. $Fe(ClO_4)_2{\cdot}6H_2O$ (0.36 g, 1 mmol) was added to obtain a violet solution, which was refluxed under argon for 0.5 h. The solution was kept overnight in the air to obtain a microcrystalline solid, which was isolated by filtration and air-dried; yield 0.27 g (≈29%). $C_{46}H_{63}O_{10}N_3Fe_2$ (929.73): C 59.43, H 6.83, N 4.52, Fe 12.01; found C 60.1, H 6.8, N 4.5, Fe 12.2. IR (KBr): $\tilde{\nu}$ = 2964, 1617, 1476, 1384, 1307, 1262, 1162, 1121, 1033, 968, 930, 857, 807 cm$^{-1}$. ESI-MS (pos. + neg. mode, $CH_3CN$ solution): *m*/*z* = 809 [M – $C_6H_{15}NH$ – $H_2O$]. X-ray quality deep purple crystals were grown from an acetonitrile solution.

**[($L^3$)$_2Fe^{III}_2$(μ-OH)$_2$] (5):** The same protocol as that for **4** was used for preparing complex **5** by replacing $H_3L^2$ with $H_2L^3$ and ferrous perchlorate with anhydrous $FeCl_2$. Deep-brown crystals were obtained from a methanol solution for the X-ray structure determination; yield 0.48 g (≈54%). $C_{48}H_{54}O_6N_4Fe_2$ (894.69): C 64.44, H 6.04, N 6.26, Fe 12.48; found C 65.0, H 6.4, N 6.2, Fe 12.3. IR (KBr): $\tilde{\nu}$ = 3642, 3441, 2991, 2913, 2853, 1607, 1572, 1474, 1445, 1384, 1324, 1310, 1294, 1265, 1161, 958, 856, 818, 802, 759, 596 cm$^{-1}$. UV/Vis in $CH_2Cl_2$: $\lambda_{max}$, nm ($\varepsilon$, $M^{-1}cm^{-1}$): 494/$6.9\times10^3$, 292 ($21.8\times10^3$).

**[($L^3$)$_2Fe^{III}_2$(μ-$OCH_3$)(μ-$OOCCH_3$)] (6):** Isolation of **6** followed the same procedure as that for **5** using anhydrous $Fe(OOCCH_3)_2$ as the metal salt. Deep violet crystals were obtained from an acetonitrile solution for X-ray structure determination; yield 0.58 g (≈61%). $C_{51}H_{58}Fe_2N_4O_7$ (950.75): calcd. C 64.43, H 6.15, N 5.89, Fe 11.75; found C 65.0, H 6.1, N 5.8, Fe 11.6. IR (KBr): $\tilde{\nu}$ = 3450, 2857, 1637, 1606, 1571, 1554, 1474, 1450, 1420, 1310, 1276, 1269, 1161, 1094, 857, 821, 803, 760 cm$^{-1}$. UV/Vis in $CH_2Cl_2$: $\lambda_{max}$, nm ($\varepsilon$, $M^{-1}cm^{-1}$): 527 ($9.6\times10^3$), 295 ($26.5\times10^3$). ESI-MS (positive mode, $CH_2Cl_2$): *m*/*z* = 877.3 [($L^3$)$_2Fe_2O$], 430 [($L^3$)Fe].

**[($L^4$)$_2Fe^{III}_2$(μ-OH)$_2$] (7):** $FeCl_2{\cdot}4H_2O$ (0.198 g, 1 mmol) was added to a solution of $H_2L^4$ (0.384 g, 1 mmol) in methanol (50 mL) under argon, resulting in a pale-brown solution, to which $Et_3N$ (0.5 mL) was added. The solution was refluxed under argon for 0.5 h, followed by stirring in the air for 1 h. The precipitated brown microcrystalline solid was separated by filtration and recrystallised twice from an acetonitrile solution to yield X-ray quality red-brown crystals of **7**·2$CH_3CN$; yield 0.4 g (40%). $C_{54}H_{78}Fe_2N_4O_6$ (990.94): calcd. C

  

65.45, H 7.93, N 5.65, Fe 11.27; found C 65.6, H 7.9, N 5.8, Fe 11.5. IR (KBr): $\tilde{\nu}$ = 3667, 3422, 2956, 2915, 2859, 1607, 1467, 1438, 1414, 1385, 1354, 1298, 1255, 1209, 1152, 1088, 1057, 1031, 926, 859, 832, 807, 626, 605 $cm^{-1}$. EI-MS: *m*/*z* (%) = 890 (15) $[(L^4)_2Fe_2O]$, 714 (100) $[(L^4)_2Fe_2O - C_{12}H_{27}]$. Complex **7** was also obtained from $Fe(ClO_4)_2{\cdot}6H_2O$ as the starting iron salt.

**$[(L^4)_2Fe^{III}_2(MeOH)(\mu\text{-}OH)(\mu\text{-}OMe)]$ (8):** Complex **8**·$CH_3OH$ was obtained from **7** through recrystallisation from a methanolic solution in presence of $[nBu_4N]OCH_3$. $C_{53}H_{82}Fe_2N_2O_8$ (986.95): calcd. C 64.50, H 8.38, N 2.84, Fe 11.32; found C 65.0, H 8.4, N 2.9, Fe 11.0. IR (KBr): $\tilde{\nu}$ = 3601, 3416, 3301, 2915, 1618, 1466, 1443, 1385, 1352, 1298, 1250, 1210, 1154, 1134, 1089, 1073, 996, 946, 924, 861, 821, 771, 600, 559 $cm^{-1}$. UV/Vis in $CH_2Cl_2$: $\lambda_{max}$, nm ($\varepsilon$, $M^{-1}cm^{-1}$): 455 ($8.3\times10^3$), 331 ($12.4\times10^3$), 283 ($24.8\times10^3$).

**X-ray Crystallographic Data Collection and Refinement of the Structures:** Single crystals for **1**, **2**, **3**·$CH_3OH$, **4**·2.5$CH_3CN{\cdot}H_2O$, **5**, **6**, **7**·2$CH_3CN$ and **8**·$CH_3OH$ were coated with perfluoropolyether, picked up with nylon loops and were mounted in the nitrogen cold stream of the diffractometer. Graphite-monochromated Mo-$K_\alpha$ radiation ($\lambda$ = 0.71073 Å) from a Mo-target rotating-anode X-ray source was used throughout. Final cell constants were obtained from least-squares fits of several thousand strong reflections. Crystal faces were determined and intensity data were corrected for absorption using the Gaussian method in SADABS.[8] Structures were readily solved by Patterson methods and subsequent difference Fourier techniques. The Siemens ShelXTL[9] software package was used for solution and artwork of the structures; ShelXL97[10] was used for the refinement. All non-hydrogen atoms were anisotropically refined and hydrogen atoms bound to carbon were placed at calculated positions and refined as riding atoms with isotropic displacement parameters. Acidic protons bound to oxygen and nitrogen atoms were located from the difference map and refined with restrained bond length and thermal displacement parameters. Split atom models were refined for disordered parts, where possible. Split positions were refined with restrained bond length, angles and thermal displacement parameters using the SADI, SAME and EADP instructions of ShelXL97. Crystallographic data of the compounds are listed in Table 8.

Table 8. Crystallographic data for **1**, **2**, **3**·$CH_3OH$, **4**·2.5$CH_3CN{\cdot}H_2O$, **5**, **6**, **7**·2$CH_3CN$, **8**·$CH_3OH$.

| | **1** | **2** | **3**·$CH_3OH$ | **4**·2.5$CH_3CN{\cdot}H_2O$ |
|---|---|---|---|---|
| Formula | $C_{32}H_{48}FeNO_5$ | $C_{34}H_{52}FeNO_5$ | $C_{40}H_{69}FeN_2O_6$ | $C_{51}H_{72.5}Fe_2N_{5.5}O_{11}$ |
| *Fw* | 582.56 | 610.62 | 729.82 | 1050.34 |
| Space group | *Iba*2, No. 45 | *Pbca*, No. 61 | $Pca2_1$, No. 29 | $P2_1/n$, No. 14 |
| *a* [Å] | 22.557(2) | 8.842(2) | 24.2976(9) | 20.1466(12) |
| *b* [Å] | 34.621(3) | 23.451(4) | 9.2462(4) | 20.2232(12) |
| *c* [Å] | 8.7112(8) | 32.700(5) | 19.3926(8) | 26.046(2) |
| $\alpha$ [°] | 90 | 90 | 90 | 90 |
| $\beta$ [°] | 90 | 90 | 90 | 96.769(2) |
| $\gamma$ [°] | 90 | 90 | 90 | 90 |
| *V* [Å] | 6803.0(10) | 6780(2) | 4356.8(3) | 10537.9(12) |
| *Z* | 8 | 8 | 4 | 8 |
| *T* [K] | 100(2) | 100(2) | 100(2) | 100(2) |
| $\rho$ calcd. [$g\,cm^{-3}$] | 1.138 | 1.196 | 1.113 | 1.324 |
| Refl. collected/$2\theta_{max}$ | 20223/44.98 | 7936/46.40 | 117967/61.96 | 134334/50.00 |
| Unique refl. with $I>2\sigma(I)$ | 4329/3279 | 3874/3162 | 13826/12943 | 18495/13153 |
| Parameters/restraints | 371/35 | 375/0 | 474/19 | 1324/17 |
| $\lambda$ [Å]/$\mu(K_\alpha)$ [$cm^{-1}$] | 0.71073/4.79 | 0.71073/4.83 | 0.71073/3.88 | 0.71073/6.13 |
| *R*1[a]/goodness of fit[b] | 0.0887/1.055 | 0.0678/1.156 | 0.0450/1.084 | 0.0462/1.053 |
| *wR*2[c] [$I>2\sigma(I)$] | 0.2251 | 0.1358 | 0.1072 | 0.0870 |
| Residual density [$e\,Å^{-3}$] | +0.66/–0.28 | +0.75/–0.44 | +0.78/–0.40 | +0.59/–0.41 |
| | **5** | **6** | **7**·2$CH_3CN$ | **8**·$CH_3OH$ |
| Formula | $C_{48}H_{54}Fe_2N_4O_6$ | $C_{51}H_{58}Fe_2N_4O_7$ | $C_{54}H_{78}Fe_2N_4O_6$ | $C_{53}H_{82}Fe_2N_2O_8$ |
| *Fw* | 894.65 | 950.71 | 990.90 | 986.91 |
| Space group | $R\bar{3}$, No. 148 | $P2_1/n$, No. 14 | $P\bar{1}$, No. 2 | $P\bar{1}$, No. 2 |
| *a* [Å] | 32.803(2) | 12.1961(6) | 10.229(2) | 11.4826(8) |
| *b* [Å] | 32.803(2) | 23.0060(13) | 11.415(2) | 13.6229(12) |
| *c* [Å] | 12.9020(8) | 16.0454(8) | 12.746(2) | 18.7220(12) |
| $\alpha$ [°] | 90 | 90 | 104.644(6) | 96.138(4) |
| $\beta$ [°] | 90 | 92.623(5) | 95.793(7) | 92.686(4) |
| $\gamma$ [°] | 120 | 90 | 101.611(7) | 112.844(4) |
| *V* [Å] | 12023.0(13) | 4690.9(4) | 1392.2(4) | 2670.9(3) |
| *Z* | 9 | 4 | 1 | 2 |
| *T* [K] | 100(2) | 100(2) | 100(2) | 100(2) |
| $\rho$ calcd. [$g\,cm^{-3}$] | 1.112 | 1.346 | 1.182 | 1.227 |
| Refl. collected/$2\theta_{max}$ | 98327/72.00 | 42197/45.00 | 27179/62.02 | 55642/62.00 |
| Unique refl. with $I>2\sigma(I)$ | 12528/9767 | 6089/3550 | 8790/7033 | 16917/14794 |
| Parameters/restraints | 278/0 | 577/0 | 311/1 | 616/3 |
| $\lambda$ [Å]/$\mu(K_\alpha)$ [$cm^{-1}$] | 0.71073/5.87 | 0.71073//6.74 | 0.71073/5.69 | 0.71073/5.95 |
| *R*1[a]/goodness of fit[b] | 0.0406/1.113 | 0.0852/1.054 | 0.0417/1.043 | 0.0473/1.162 |
| *wR*2[c] [$I>2\sigma(I)$] | 0.0823 | 0.1529 | 0.0895 | 0.1214 |
| Residual density [$e\,Å^{-3}$] | +0.55/–0.55 | +0.77/–0.50 | +0.46/–0.29 | +1.25/–0.62 |

[a] Observation criterion: $I>2\sigma(I)$. $R1 = \Sigma||F_o| - |F_c||/\Sigma|F_o|$. [b] GooF = $\{\Sigma[w(F_o^2 - F_c^2)(n-p)]\}^{1/2}$. [c] $wR2 = \{\Sigma[w(F_o^2 - F_c^2)^2]/\Sigma[w(F_o^2)^2]\}^{1/2}$, where $w = 1/\sigma^2(F_o^2) + (aP)^2 + bP$, $P = (F_o^2 + 2F_c^2)/3$.

  

CCDC numbers 805368 (for **1**), 805369 (for **2**), 805370 (for **3**), 805371 (for **4**), 805372 (for **5**), 805373 (for **6**), 805374 (for **7**) and 805375 (for **8**) contain the supplementary crystallographic data for this paper. These data can be obtained free of charge from the Cambridge Crystallographic Data Centre via www.ccdc.cam.ac.uk/data_request/cif.

**Supporting Information** (see footnote on the first page of this article): Figures S1 and S2 contain the molecular structures and Tables S1 and S2 selected bond lengths and angles for **1** and **2**. Details of the magnetic SQUID measurements are also included.

## Acknowledgments

Financial support from the Max-Planck-Gesellschaft is gratefully acknowledged. Thanks are also due to Ms. H. Schucht, Mr. U. Pieper and Mr. A. Göbels for skilful technical assistance.

[1] For selected examples, see: a) R. H. Holm, E. I. Solomon, *Chem. Rev.* **2004**, 104; b) J. Stubbe, W. A. van der Donk, *Chem. Rev.* **1998**, *98*, 705; c) J. A. Halfen, B. A. Jazdzewski, S. Mahapatra, I. M. Berreau, E. C. Wilkinson, L. Que Jr., W. B. Tolman, *J. Am. Chem. Soc.* **1997**, *119*, 8217; d) Y. Wang, T. D. P. Stack, *J. Am. Chem. Soc.* **1996**, *118*, 1309; e) E. Bill, J. Müller, T. Weyhermüller, K. Wieghardt, *Inorg. Chem.* **1999**, *38*, 5795; f) S. Itoh, S. Takayama, R. Arakawa, A. Furuta, M. Kumatsu, A. Ishida, S. Takamuku, S. Fukuzumi, *Inorg. Chem.* **1997**, *36*, 1407; g) D. Zurita, I. Gautier-Luneau, S. Menage, J. L. Pierre, E. Saint-Aman, *J. Biol. Inorg. Chem.* **1997**, *2*, 46; h) P. Chaudhuri, K. Wieghardt, *Prog. Inorg. Chem.* **2001**, *50*, 151.

[2] See, for example: a) O. Kahn, *Molecular Magnetism*, VCH Publishers, New York, **1993**; b) G. Christou, D. Gatteschi, D. N. Hendrickson, R. Sessoli, *MRS Bull.* **2000**, *25*, 66; c) C. J. O'Connor (Ed.), *Research Frontiers in Magnetochemistry*, World Scientific, Singapore, **1993**; d) O. Kahn, *J. Solid State Chem.* **2001**, *159*.

[3] a) G. J. P. Britovsek, V. C. Gibson, D. F. Wass, *Angew. Chem. Int. Ed.* **1999**, *38*, 428; b) F. Bonnet, A. R. Cowley, P. Mountford, *Inorg. Chem.* **2005**, *44*, 9046; c) E. Y. Tshuva, M. Versano, I. Goldberg, M. Kol, H. Weitman, Z. Goldschmidt, *Inorg. Chem. Commun.* **1999**, *2*, 371; d) I. P. Rothwell, *Acc. Chem. Res.* **1988**, *21*, 153; e) Y. Chen, S. Yekta, A. K. Yudin, *Chem. Rev.* **2003**, *103*, 3155; f) R. R. Schrock, A. H. Hoveyda, *Angew. Chem. Int. Ed.* **2003**, *42*, 4592.

[4] N. V. Timosheva, A. Chandrasekharan, R. O. Day, R. R. Holmes, *Inorg. Chem.* **1998**, *37*, 4945.

[5] a) E. Y. Ishuva, I. Goldberg, M. Kol, *J. Am. Chem. Soc.* **2000**, *122*, 10706; b) A. van der Linden, C. J. Schaverien, N. Neijboom, C. Ganter, A. G. Orpen, *J. Am. Chem. Soc.* **1995**, *117*, 3008; c) E. B. Tjaden, D. C. Swenson, R. F. Jordan, J. L. Petersen, *Organometallics* **1995**, *14*, 371; d) L. M. G. Thorn, Z. C. Etheridge, P. E. Fanwick, I. P. Rothwell, *Organometallics* **1998**, *17*, 3636; e) Y. Nakayama, K. Watanabe, N. Ueyama, A. Nakamura, A. Harada, J. Okuda, *Organometallics* **2000**, *19*, 2498; f) J. Okuda, S. Fokken, T. Kleinhenn, T. P. Spaniol, *Eur. J. Inorg. Chem.* **2000**, 1321; g) E. Y. Tshuva, I. Goldberg, M. Kol, Z. Goldschmidt, *Organometallics* **2001**, *20*, 3017.

[6] a) T. Weyhermüller, T. K. Paine, E. Bothe, E. Bill, P. Chaudhuri, *Inorg. Chim. Acta* **2002**, *337*, 344; b) T. K. Paine, T. Weyhermüller, E. Bill, E. Bothe, P. Chaudhuri, *Eur. J. Inorg. Chem.* **2003**, 4299; c) T. K. Paine, E. Rentschler, T. Weyhermüller, P. Chaudhuri, *Eur. J. Inorg. Chem.* **2003**, 3167; d) P. Chaudhuri, R. Wagner, S. Khanra, T. Weyhermüller, *Dalton Trans.* **2006**, 4962; e) P. Chaudhuri, R. Wagner, T. Weyhermüller, *Inorg. Chem.* **2007**, *46*, 5134; f) E. Safaei, T. Weyhermüller, E. Bothe, K. Wieghardt, P. Chaudhuri, *Eur. J. Inorg. Chem.* **2007**, 2334.

[7] a) J. G. Wilson, *Aust. J. Chem.* **1990**, *43*, 1283; b) T. Toupance, S. R. Dubberley, N. H. Rees, B. R. Tyrell, P. Mountford, *Organometallics* **2002**, *21*, 367; c) M. M. Whittaker, W. R. Duncan, J. W. Whittaker, *Inorg. Chem.* **1996**, *35*, 382.

[8] *SADABS*, version 2006/1, Bruker Area Detector Absorption and Other Correction, G. M. Sheldrick, University of Göttingen, Germany, **2006**.

[9] *ShelXTL* 6.14 Bruker AXS Inc., Madison, WI, USA **2003**.

[10] *ShelXL97*, G. M. Sheldrick, University of Göttingen, Germany, **1997**.

[11] K. Nakamoto, *Infrared and Raman Spectra of Inorganic Compounds*, 5th ed., Wiley-Interscience, NY **1997**.

[12] A. W. Addison, T. N. Rao, J. Reedijk, J. van Rijn, G. C. Verschoor, *J. Chem. Soc., Dalton Trans.* **1984**, 1349.

[13] D. Moon, M. S. Lah, R. E. D. Sesto, J. S. Miller, *Inorg. Chem.* **2002**, *41*, 4708, and references cited therein.

[14] a) M. Kato, Y. Yamada, T. Inagaki, W. Mori, K. Sakai, T. Tsubomura, M. Sato, S. Yano, *Inorg. Chem.* **1995**, *34*, 2645; b) P. N. Turaski, W. H. Armstrong, S. Liu, S. N. Brown, S. J. Lippard, *Inorg. Chem.* **1994**, *33*, 636.

[15] E. Bill, *Julx Program*, Max-Planck-Institut für Bioanorganische Chemie, Mülheim an der Ruhr, Germany, **2005**.

[16] A. J. Blake, C. M. Grant, S. Parsons, G. A. Solan, R. E. P. Winpenny, *J. Chem. Soc., Dalton Trans.* **1996**, 321.

[17] F. L. Gall, F. Fabrizi, A. Caneschi, P. Cinelli, A. Cornia, A. C. Fabretti, D. Gatteschi, *Inorg. Chim. Acta* **1997**, *262*, 123.

[18] S. Kawata, M. Nakamura, Y. Yamashita, K. Asai, K. Kikuchi, I. Ikemoto, M. Kadata, H. Sano, *Chem. Lett.* **1992**, 135.

[19] M. A. Alam, M. Nethaji, M. Ray, *Inorg. Chem.* **2005**, *44*, 1302.

[20] B. P. Murch, F. C. Bradley, P. D. Boyle, V. Papaefthymion, L. Que Jr., *J. Am. Chem. Soc.* **1987**, *109*, 7993.

[21] G. D. Fallon, A. Markiewicz, K. S. Murray, T. Quach, *J. Chem. Soc., Chem. Commun.* **1991**, 198.

[22] K. Spartalian, J. A. Bonadies, C. J. Carrano, *Inorg. Chim. Acta* **1988**, *152*, 135.

[23] B. Chiari, O. Piovesana, T. Tarantelli, P. F. Zanazzi, *Inorg. Chem.* **1983**, *22*, 2781.

[24] B. Chiari, O. Piovesana, T. Tarantelli, P. F. Zanazzi, *Inorg. Chcem.* **1982**, *21*, 2444.

[25] J. A. Bertrand, P. G. Eller, *Inorg. Chem.* **1974**, *13*, 927.

[26] A. Neves, L. M. Rossi, I. Vencato, W. Haase, R. Werner, *J. Chem. Soc., Dalton Trans.* **2000**, 707.

[27] A. Elmali, Y. Elerman, I. Svoboda, *Z. Naturforsch., Teil B* **2001**, *56*, 897.

[28] T. Weyhermüller, R. Wagner, P. Chaudhuri, *Inorg. Chim. Acta* (**2011**), in the press.

[29] B. S. Snyder, G. S. Patterson, A. J. Abrahamson, R. H. Holm, *J. Am. Chem. Soc.* **1989**, *111*, 5214.

[30] S. Mukherjee, T. Weyhermüller, E. Bothe, P. Chaudhuri, *Eur. J. Inorg. Chem.* **2003**, 1956.

[31] P. Chaudhuri, M. Winter, K. Wieghardt, S. Gehring, W. Haase, B. Nuber, J. Weiss, *Inorg. Chem.* **1988**, *27*, 1564.

[32] For a long list of compounds, see: R. Werner, S. Ostrovsky, K. Griesar, W. Haase, *Inorg. Chim. Acta* **2001**, *326*, 78.

[33] P. W. Anderson, *Solid State Phys.* **1963**, *14*, 25.

[34] a) S. M. Gorun, S. J. Lippard, *Inorg. Chem.* **1991**, *30*, 1625; b) H. Weihe, H. U. Güdel, *J. Am. Chem. Soc.* **1997**, *119*, 6539.

Received: December 21, 2010
Published Online: April 28, 2011

  